Science of the Total Environment 911 (2024) 168616

Contents lists available at ScienceDirect

Science of the Total Environment

journal homepage: www.elsevier.com/locate/scitotenv

Photochemical reactivity of water-soluble dissolved organic matter from microplastics and microfibers

Mitchell M. Schutte [a,b], Shimaa M. Kteeba [a,c], Laodong Guo [a,*]

[a] School of Freshwater Sciences, University of Wisconsin-Milwaukee, 600 E. Greenfield Ave., Milwaukee, WI 53204, USA
[b] Milwaukee Metropolitan Sewerage District, 260 W. Seeboth Street, Milwaukee, WI 53204, USA
[c] Faculty of Science, Damietta University, New Damietta 34511, Damietta, Egypt

HIGHLIGHTS

- Water-soluble DOM yields of seven pristine MPs and three MFs were evaluated.
- Microfibers yielded much higher DOM than microplastics.
- DOM yields and properties are related to inherent polymer structure and morphology.
- MFs-derived DOM is smaller-size, highly negatively charged, and less photoreactive.
- Degradation rate constants of plastic-derived DOM are plastic or polymer specific.

GRAPHICAL ABSTRACT

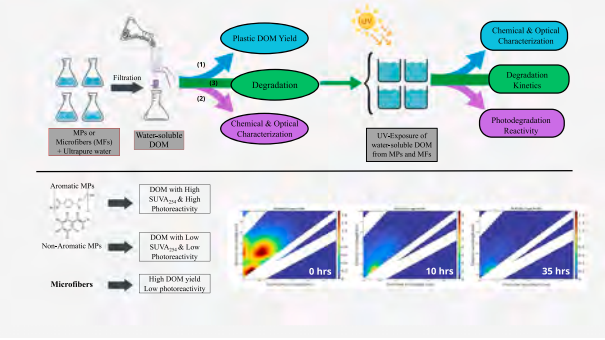

ARTICLE INFO

Editor: Damia Barcelo

Keywords:
Microfibers
Microplastics
Dissolved organic matter
Photochemical degradation
Degradation kinetics
Environmental fate

ABSTRACT

Plastics in aquatic environments are a source of dissolved organic matter (DOM). However, its production pathways and environmental fate remain poorly understood. This study investigated the yields, characterization, and photochemical reactivities of water-soluble DOM from seven pristine microplastics (MPs) and three microfibers (MFs). We found yields of plastic-derived DOM per unit mass of MPs or MFs, including chromophoric DOM (CDOM) and dissolved organic carbon (DOC), were significantly influenced by polymer chemical structures. Notably, MFs exhibited consistently higher DOM yields compared to MPs. In addition, plastics containing aromatic rings, such as PETE and PS, were found to generate higher CDOM yields, although PVC also showed elevated CDOM yields. The plastic-derived DOM had a diverse molecular size-range, spanning from 60 nm (polyester-DOM) to 937 nm (LDPE-DOM), while Zeta potentials, which were predominantly negatively charged, varied from −42.5 mV (nylon-DOM) to +4.6 mV (LMW-PVC-DOM). Degradation rate constants for CDOM (0.001–0.022 h^{-1}) were generally higher than DOC (0.0009–0.020 h^{-1}), with a shorter half-life for PETE- and PS-derived DOM. The reactivity and degradation kinetics of plastic-derived DOM were notably manifested in changes of fluorescence spectra (excitation-emission matrixes) during photochemical weathering, showing the influence of polymeric composition/structures. This baseline study provides an improved understanding of the characterization and environmental fate of microfiber- and plastic-derived DOM in aquatic environments.

* Corresponding author.
E-mail address: guol@uwm.edu (L. Guo).

https://doi.org/10.1016/j.scitotenv.2023.168616
Received 16 August 2023; Received in revised form 14 November 2023; Accepted 14 November 2023
Available online 20 November 2023

1. Introduction

Global plastic production is predicted to hit 1100 million tons (Mt) by 2050, with much of it continuing to reach waterways and further disrupt ecosystems (Ateia et al., 2022; Forum and Company, 2016; Geyer et al., 2017; Hendrickson et al., 2018; Kanhai et al., 2020; OECD, 2022). Plastics are being found not only in marine and freshwater environments but also in polar regions (Cózar et al., 2017; Eerkes-Medrano et al., 2015; Lenaker et al., 2021; Napper and Thompson, 2020), as well as in fish and human blood samples (Leslie et al., 2022; Piyawardhana et al., 2022). In aquatic systems, plastics will eventually fragment and degrade, leading to the production of dissolved organic matter (DOM) and secondary microplastics (MPs) and nanoplastics (Gillibert et al., 2019; Lim, 2021; van Wezel et al., 2016). Aside from the negative effects of plastic debris and MPs on the environment and aquatic organisms (Ahmed et al., 2023; Stubbins et al., 2021), plastic-derived DOM also impacts environmental and biogeochemical processes (Chen et al., 2022; Lee et al., 2021; Romera-Castillo et al., 2018). Recent studies have shown that photodegradation of plastic-derived DOM can produce low molecular weight, biologically active DOC (Gewert et al., 2018; Zhu et al., 2020), which can complex with metals (Lee et al., 2021), slow organic pollutant degradation (Chen et al., 2022), and stimulate microbial activity in the ocean (Romera-Castillo et al., 2018). Zhu et al. (2020) suggest that the DOM leached from MPs may be readily available for degradation and involved in biogeochemical processes. The amount of DOM leached from these MPs is thought to be higher than previously hypothesized. Romera-Castillo et al. (2018) estimated that up to 23,600 metric tons of plastic DOC may leach from plastic polymers of mixed sources and commercially available packaging into the oceans annually, comprising a substantial portion of the ocean's carbon pool.

Many previous studies have utilized commercial plastics in their investigations, which are known to contain a variety of additives (Lee et al., 2020; Sun et al., 2022). Although some studies have highlighted the impact of plastic composition and additives on DOM leaching for a limited range of plastic types, there are few systematic studies on the release potential of water-soluble DOM from all major MPs and microfibers (MFs). The scarcity of studies evaluating the yields of water-soluble DOM between MPs and MFs is particularly concerning since MFs are the most prevalent MPs in aquatic environments (Gago et al., 2018; Singh et al., 2020; Gunaalan et al., 2023).

Besides evaluating the production of water-soluble DOM from plastics, it is crucial to characterize plastic derived DOM and delineate their reactivity and environmental fate. A few recent studies have examined microbial consumption and photodegradation of DOM released from selected MPs (Lee et al., 2020; Romera-Castillo et al., 2022). However, reports on the chemical characterization of plastic DOM remain limited and are mostly on a few select plastics (Boldrini et al., 2021; Lee et al., 2020). The photochemical reactivity, degradation kinetics and environmental fate of water-soluble DOM from both MPs and MFs remain largely unexplored.

This study aimed to enhance the understanding of the often-neglected consequences of plastic pollution by investigating the characterization and photochemical reactivity of plastic-derived DOM. The major objectives were to: 1) investigate the water-soluble DOM yields from major plastic polymers, including seven MPs and three MFs in freshwater environments, 2) characterize optical and chemical properties of plastic-derived DOM from pristine MPs and MFs, and 3) uncover the photochemical reactivity and degradation kinetics of plastic-derived DOM, including both chromophoric DOM (CDOM) and dissolved organic carbon (DOC), in response to UV light exposure. The results highlight the substantial leached DOM yield of pristine microplastics/microfibers and the selective photodegradation of plastics-derived DOM containing aromatic functional groups.

2. Materials and methods

2.1. Plastic leaching experiments

Leaching experiments were performed to evaluate the yields of water-soluble DOM, per mass of plastic in grams, from different plastic polymers and selected MFs and to obtain plastic-derived DOM for further degradation experiments (Table 1 and Fig. 1). Seven MPs, including polyethylene terephthalate (PETE), high density polyethylene (HDPE), low molecular weight (LMW)-polyvinyl chloride (LMW-PVC), high molecular weight-PVC (HMW-PVC), low density polyethylene (LDPE), polypropylene (PP), polystyrene (PS); and three MFs, including polyester (PES), nylon (NYL), and cellulose (CE), were utilized. Detailed information, including CAS #, source, and polymer properties, of MPs and MFs are listed in Table 1.

Pre-determined amounts (masses) of polymers were placed in acid-cleaned glass beakers with 100 mL of ultrapure water for 2 days with intermittent shaking. Similar weight/volume (*W/V*) ratios of plastic/water were used (Table 1). These specific W/V ratios were found to be optimal for generating water-soluble DOM for further degradation experiments. The leachates were filtered through pre-combusted (at 500 °C) glass fiber filters (GF/F, Whatman, 0.7 μm). The filtrate was collected, and the plastic beads and MFs were saved for a second leaching. The steps above were then repeated, and leachates of each plastic type were combined. All samples were stored covered, without exposure to light sources until analyses or degradation experiments.

2.2. Photodegradation of plastic-derived DOM

Plastic-derived DOM samples from PETE, LMW-PVC, PS and NYL were evaluated for the photochemical degradation experiments to assess their degradation kinetics and photochemical reactivity. Plastics were selected due to their differing molecular characteristics, particularly the presence or absence of aromatic components, and their ability to produce adequate DOM yields during initial leaching tests.

Plastic-derived DOM was placed in a pre-combusted (550 °C) glass beaker covered with a quartz lid for photochemical degradation using a 400 W UV lamp (MH1-400 EB) with a measured irradiance 850 W m^{-2}. During photodegradation, time-series samples (up to 110 h) were taken for measurements of bulk dissolved organic carbon (DOC), chromophoric DOM (CDOM), including UV-absorption spectra and fluorescence excitation-emission matrix (EEM), and other chemical properties. Ultrapure water was added prior to sampling to account for any evaporation during degradation (Walsh et al., 2021). Replicate experiments were conducted and the mean values with standard deviation were presented.

2.3. Measurements of CDOM, DOC, and fluorescence EEM

UV–vis spectrophotometry (Agilent 8453) with a 1 cm quartz cuvette was used to measure absorption spectra between 190 and 1100 nm with 1 nm increments (DeVilbiss et al., 2016; Zhou et al., 2016). Blanks were subtracted from absorbances by scanning ultrapure water prior to sample analyses. Absorption coefficients, α_{254} (m^{-1}) representing CDOM, were converted from UV-absorbance at 254 nm (A) as $a_{254} = 2.303\,A/l$, where l is the cuvette path length in meters.

Concentrations of DOC were measured using a Shimadzu TOC analyzer (TOC-L). Samples were acidified to pH $\leq$ 2 and sparged with zero air before measurements. Ultrapure water, working standards, and certified DOC standard (from University of Miami) were frequently run as samples to ensure DOC data quality (Zhou et al., 2016). Analytical precision in terms of coefficient of variation (CV) was 2 % or better.

Fluorescence excitation-emission matrices (EEMs) of DOM samples were measured on a Shimadzu spectrofluorometer (RF-6000) and a 1 cm path-length quartz cuvette. The emission (Em) spectra were scanned from 280 to 600 nm with 2 nm intervals under the excitation wavelength

(Ex) ranging from 250 to 480 nm with 5 nm intervals. The instrument was set at a scanning speed of 6000 nm/min and a bandwidth of 5.0 nm. Before sample measurements, ultrapure water was measured as a blank (Lin and Guo, 2020; Zhou et al., 2013).

2.4. Other optical properties

Values of specific UV absorbance at 254 nm ($SUVA_{254}$) were calculated as the ratio of A_{254} to DOC concentration (mg-C L^{-1}) to gauge the apparent aromaticity of samples (Weishaar et al., 2003). Characteristics of the absorbance spectra were evaluated at 275–295 nm ($S_{275–295}$) to calculate spectral slopes using linear regression of log fitted absorption coefficients (DeVilbiss et al., 2016; Helms et al., 2008).

Based on fluorescence EEM data, humification index (HIX), indicating the extent of humification of DOM, and biological index (BIX), were calculated (Huguet et al., 2009; Lin et al., 2021).

2.5. Surface properties

Changes in colloidal and surface properties, including zeta potential and molecular sizes of plastic-derived DOM, were evaluated using a Zetasizer (Malvern, Nano ZS). Standard PS-Latex nanoparticles with known mode size of 100 nm were used as samples to check instrument performance ($\mu = 97.98$ nm, $\sigma = 0.79$, RSD = 0.81 %, $n = 9$) as done in (Kteeba et al., 2017).

2.6. Statistical analyses

All statistical analyses for comparisons and correlations were completed in R version 4.2.3 using the ggplot2, ggpmisc, ggpubr, and rstats packages. One-way ANOVA was used for comparison of plastic-derived DOM yields between MFs and MPs. Welch's *t*-test was used to determine the significance between surface properties of initial and degraded samples. Significance levels with *p*-value <0.05 were selected for all statistical analyses.

3. Results and discussion

3.1. Water-soluble DOM yields from different plastic polymers

Leaching experiments were conducted on pristine MPs and MFs exposed to ultrapure water to determine the yield of water-soluble DOM, including CDOM and DOC, and to obtain plastic-derived DOM for degradation experiments. The water-soluble DOM yields per unit mass of plastics were significantly higher in MFs, leaching a magnitude of 10–1000 times more DOM than the selected MPs. This was especially apparent in nylon (NYL) compared to MPs (Fig. 1). For example, yields of CDOM and DOC from MFs ranged from 0.27 to 5.5 a.u. CDOM/g-MF and 1.1–11.7 mg-DOC/g-MF, while DOM yields from MPs were 3.7×10^{-3} – 3.2×10^{-2} a.u. CDOM/g-MP and 2.5×10^{-3} – 1.0×10^{-1} mg DOC/g -MPs, respectively.

Among the MPs assessed, PETE, PVC, including both LMW-PVC and HMW-PVC, and PS had significantly higher DOM yields per unit mass of plastic ($p = 0.048$ for CDOM and $p = 0.008$ for DOC) compared to HDPE,

Table 1
List of polymers (microplastics and microfibers) used and their chemical properties. MF deniers are 2.0 for polyester and 1.0 for Nylon 66, both are mini fibers.

Polymer	Short Name	Form	CAS No.	Source	Chemical Formula	Monomer Structure	Molar Mass (g/mol)	W:V Ratio (g/L)
Polyethylene terephthalate	PETE	Granule	25038-59-9	Sigma-Aldrich	$(C_{10}H_8O_4)_n$	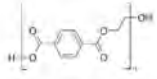	192.7	50
High density polyethylene	HDPE	Granule	9002-88-4	Sigma-Aldrich	$H(CH_2CH_2)_nH$		28.05	50
Low MW Polyvinyl chloride	LMW-PVC	Powder	9002-86-2	Sigma-Aldrich	$(CH_2CHCl)_n$	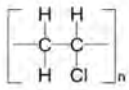	62.4	50
High MW Polyvinyl chloride	HMW-PVC	Powder	9002-86-2	Sigma-Aldrich	$(CH_2CHCl)_n$		62.4	12.5
Low density polyethylene	LDPE	Granule	9002-88-4	Sigma-Aldrich	$H(CH_2CH_2)_nH$		28.05	50
Polypropylene	PP	Granule	9003-07-0	Sigma-Aldrich	$[CH_2CH(CH_3)]_n$		42.08	50
Polystyrene	PS	Granule	9003-53-6	Sigma-Aldrich	$[CH_2CH(C_6H_5)]_n$		118.2	50
Polyester	PES	Fiber	-	Testfabrics Inc.	$(C_{10}H_8O_4)_n$		192.7	10
Nylon 66	NYL	Fiber	-	Testfabrics Inc.	$(C_{12}H_{22}N_2O_2)_n$	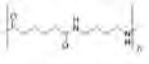	226.32	10
Cellulose	CE	Fiber	9004-34-6	Sigma-Aldrich	$(C_6H_{10}O_5)_n$		162.14	10

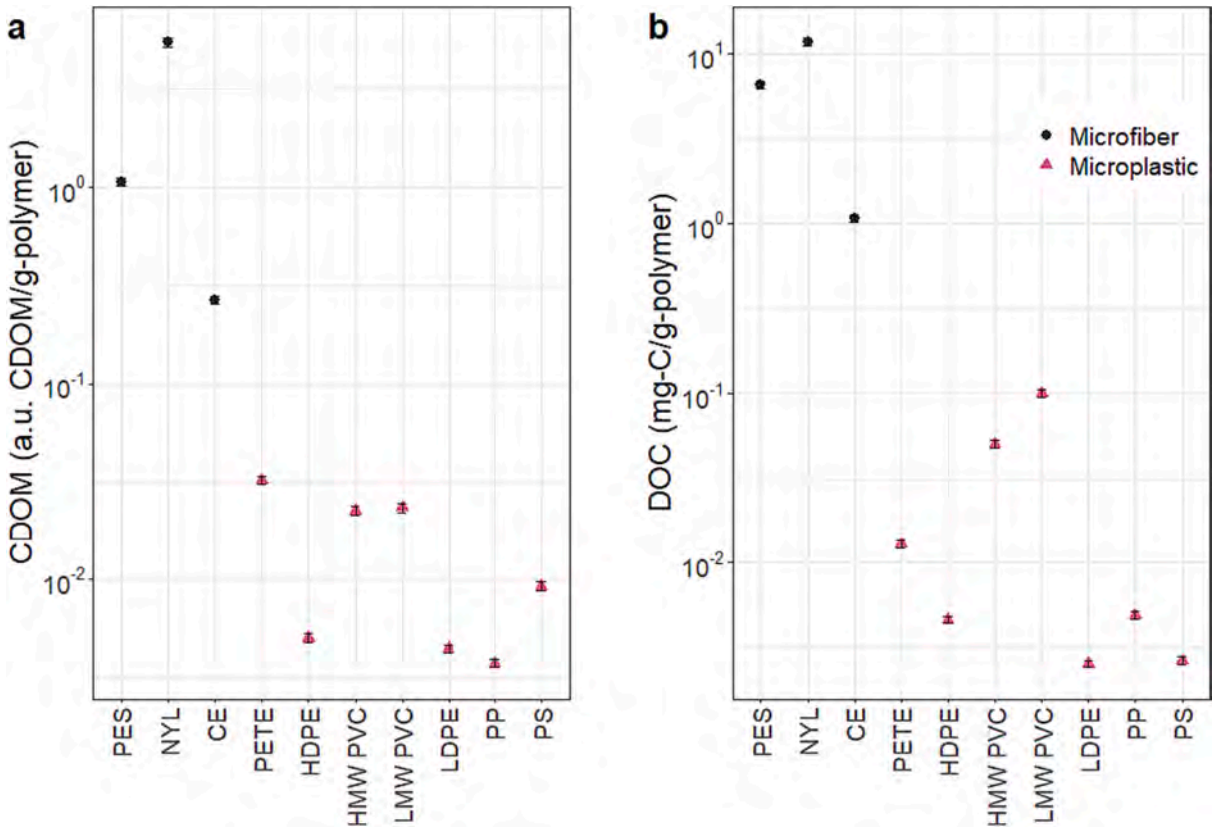

Fig. 1. Yields of CDOM (a) and DOC (b) from pristine microfibers (MFs, including polyester, PES, nylon, NYL, and cellulose, CE) and seven microplastics (MPs, including polyethylene terephthalate (PETE), high density polyethylene (HDPE), low molecular weight-polyvinyl chloride (LMW-PVC), high molecular weight-PVC (HMW-PVC), low density polyethylene (LDPE), polypropylene (PP), and polystyrene (PS)), showing higher CDOM yields from selected MFs, plastic polymers containing aromatic rings, such as PETE and PS, and PVC and higher DOC yields from MFs, PVC, and PETE. Results are averages of three sample replicates with error bars.

LDPE, and PP. The lowest CDOM yield was observed for PP and the lowest DOC yield was observed for LDPE (Fig. 1). PETE and PS polymers had considerably higher CDOM yields than DOC yields compared to other polymers, consistent with the occurrence of aromatic functionalities or photochemical responsive groups in both PETE and PS structures (Table 1). With exception for PVC polymers, all MPs with C—C backbones, such as PP, HDPE, and LDPE, exhibited low DOM yields when exposed solely to ultrapure water (Fig. 1). In contrast, MPs and MFs that contain heteroatoms like ester or amide bonds leached far higher yields. These observations agree well with those reported previously for polymer degradation (Gewert et al., 2015). Both HMW- and LMW-PVC leached large amounts of DOM, indicating chloride bonds in the chemical structure may be an important degradation function during hydrolysis. While PVC does not have an aromatic component, the initial polymerization of PVC introduces diene and triene compounds into the structure that act as chromophores (Decker, 1984). This may explain the high CDOM yields from PVC observed here.

Lee et al. (2020) conducted leaching experiments on MPs using artificial freshwater for a duration of 7 days, employing plastic concentrations ranging from 1 to 5 g per liter of PVC or PS. Their findings align with our results, particularly in the case of PVC, which yielded approximately 0.1 mg of carbon per gram of PVC. However, our data indicated substantially lower levels of DOC produced from PS. This is a possible indication that dissolved ions act to enhance MP leaching in freshwaters due to complex formation and changes in surface charges. However, an existing study conducted by Cai et al. (2018), has previously reported that UV exposure in high salinity artificial seawater (56 ppt) induces less polymer degradation compared to exposure in air or ultrapure water. The contrast between freshwater and seawater is likely due to increased ionic strength of sea water which could inhibit leaching. Further research is needed to thoroughly investigate this disparity and to determine the specific mechanisms involved.

Among the MF samples, NYL produced the highest DOM yield, followed by PES and CE. The physical structure of the NYL and PES are similar, with PES having a thicker fiber weave (denier = 2). Even in a powdered form, with a high surface area to volume ratio, the DOM yields of CE are lower than other MFs (NYL and PES) although higher than MPs. Interestingly, PES has a reactive oxygen group in its structure but resulted in lower CDOM and DOC yields than NYL (Fig. 1). However, NYL may also contain an aromatic group, such as aromatic diacids-containing polyphthalamide in nylon's polymer chain (Park et al., 2014; Weber, 2011), resulting in highest CDOM and DOC yields per unit mass of plastic compared to other MFs (Fig. 1).

3.2. Optical characterization of plastic DOM

Differences in optical properties, including $SUVA_{254}$ and spectral slope in the 275–295 nm range ($S_{275–295}$), in initial water-soluble DOM among plastic polymers are shown in Fig. 2. $SUVA_{254}$ values for plastic-derived DOM ranged from 0.0007 to 0.015 L mg^{-1} m^{-1}, with the highest values in DOM derived from PS and PETE, followed by LDPE, HDPE, and PP. $SUVA_{254}$ values were low for both forms of PVC. Water-soluble DOM derived from MFs, including polyester (PES), NYL and cellulous (CE), had low $SUVA_{254}$ values compared to MPs (Fig. 2a). As expected, and like CDOM yields, $SUVA_{254}$ were highest for MPs, such as PS and PETE, containing aromatic rings in their chemical structure (Table 1) although PVC was an exception to this relationship (Figs. 1 and 2). In addition to its highest CDOM yield from MFs, water-soluble DOM from NYL had the

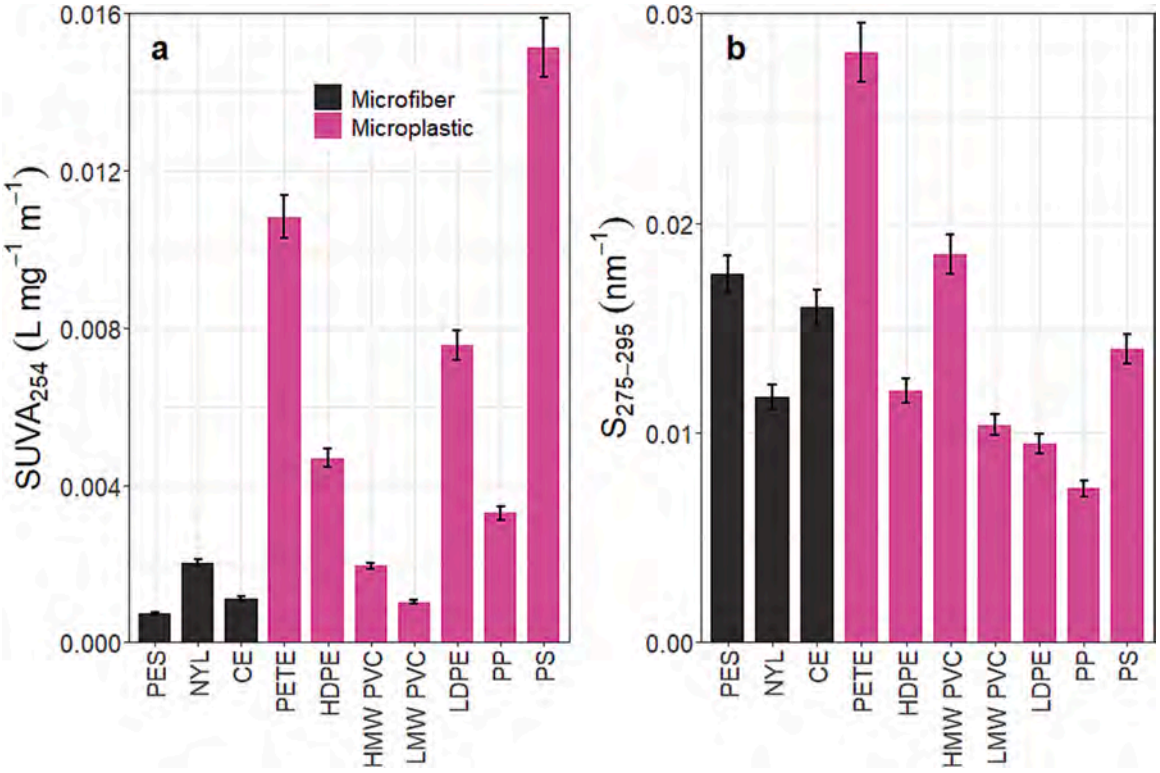

Fig. 2. Variations in optical properties of water-soluble DOM released from different MFs and MPs, including (a) specific UV absorbance at 254 nm ($SUVA_{254}$) and (b) spectral slope value between 275 and 295 nm ($S_{275–295}$). Results are averages of three sample replicates.

highest $SUVA_{254}$ value among MFs, but not as high as those aromatic-containing MPs (Fig. 2). Overall, the results indicate a potential for MP-derived DOM to be more photoreactive than MF-derived DOM in most common polymer types although, no significant correlation was observed between $SUVA_{254}$ values and CDOM yields in this study.

The variation in spectral slope ($S_{275–295}$) or apparent DOM molecular weights among polymers is depicted in Fig. 2b. DOM samples from selected MFs had $S_{275–295}$ values increasing or molecular weight decreasing from NYL to CE and PES. This variation trend in DOM spectral slope or apparent molecular weight did not closely follow trends in fiber's molecular mass (226 g/mol for NYL, 192 for PES, and 162 for CE, Table 1). This is likely due to the difference in shape and size between CE (powered) and mini fibers (NYL and PES). Among DOM samples from MPs, values of $S_{275–295}$ were highest in PETE, PS, and HMW-PVC, followed by HDPE, LMW-PVC, LDPE, and PP. Similar to MFs, $S_{275–295}$ values among MP-derived DOM did not have a correlation with the molecular mass of their corresponding polymers (Table 1). Instead, higher $S_{275–295}$ values or lower DOM molecular weights were observed in plastic-derived DOM from MPs with higher CDOM yields and those containing aromatic groups (e.g., PETE and PS) with exception of HMW-PVC (Fig. 2b). MPs with lower CDOM yields, such as HDPE, LDPE, and PP, produced water-soluble DOM with lower $S_{275–295}$ values or higher DOM molecular weight, except for LMW-PVC. These results suggest that, compared to MFs, both CDOM yields and DOM molecular weight, are mostly associated with polymer's functionalities and less related to polymer's molecular mass. In addition, some water-soluble plastic DOM may not contain monomers from their corresponding polymers and subsequent DOM coagulation/aggregation could occur after release from plastic surfaces.

3.3. Fluorescence characterization of plastic-derived DOM

In addition to CDOM, plastic-derived DOM were characterized using fluorescence spectroscopy. Examples of the fluorescence EEM spectra for plastic-derived DOM from NYL, LMW-PVC, PETE, PP, and PS are shown in Fig. 3. Major fluorescence peaks in the initial (0 h) water-soluble DOM samples from selected polymers included those at Ex/Em of 325/425 nm, 275/325 nm, and 250/400 nm, which are similar to peak-C, peak-T and peak-A reported for natural DOM. Peak-A, with its Ex/Em maximum at 250/400 nm, is indicative of the presence of humic substances and suggests the presence of complex, high-molecular-weight organic matter. Peak-C, at Ex/Em ≈ 325/425 nm, is often attributed to humic-like or visible terrestrial humic-like DOM components, while Peak-T, located at Ex/Em ≈ 275/325 nm, is associated with tyrosine-like and protein-like fluorophores (Coble, 2007; Osburn et al., 2011; Zhou et al., 2013). While water soluble DOM from aromatic polymer PS exhibited all major fluorescence peaks (Peaks A, C, and T), DOM from PETE, also containing an aromatic group, did not show significant fluorescence intensities in Peaks A and C. On the other hand, water soluble DOM from LMW-PVC, which contains no aromatic group, also exhibited all major fluorescence peaks (A, C, and T), which is unexpected. Peak T has previously been reported in leached DOM for PS and PVC (Lee et al., 2020), but their DOM samples also exhibited Peak B (~225(~280)/~305 nm) which was absent in these samples. In addition to PS and LMW-PVC, NYL-derived DOM also contained humic-like Peaks A and C, which agrees well with its higher CDOM yield and aromaticity shown in Figs. 1 and 2, and likely related to the presence of aromatic diacids-containing polyphthalamide in nylon's polymer chain (Park et al., 2014; Weber, 2011). Generally, plastic-derived DOM fluorophores released from NYL, LMW-PVC, PETE, PP, and PS followed closely to their CDOM yields (per unit mass of plastics) and inherent polymer structures. The DOM released from these polymers had a range of EEM spectra with different major fluorescence peaks similar to peaks C, A, and T.

Within the selected polymers, PS- and PVC-derived DOM had the highest HIX value followed by NYL and PETE, while PP had the lowest HIX value (Table S1). The higher HIX values observed for DOM released from PS, PVC, and NYL are consistent to their diverse fluorescence spectra and higher $SUVA_{254}$ values.

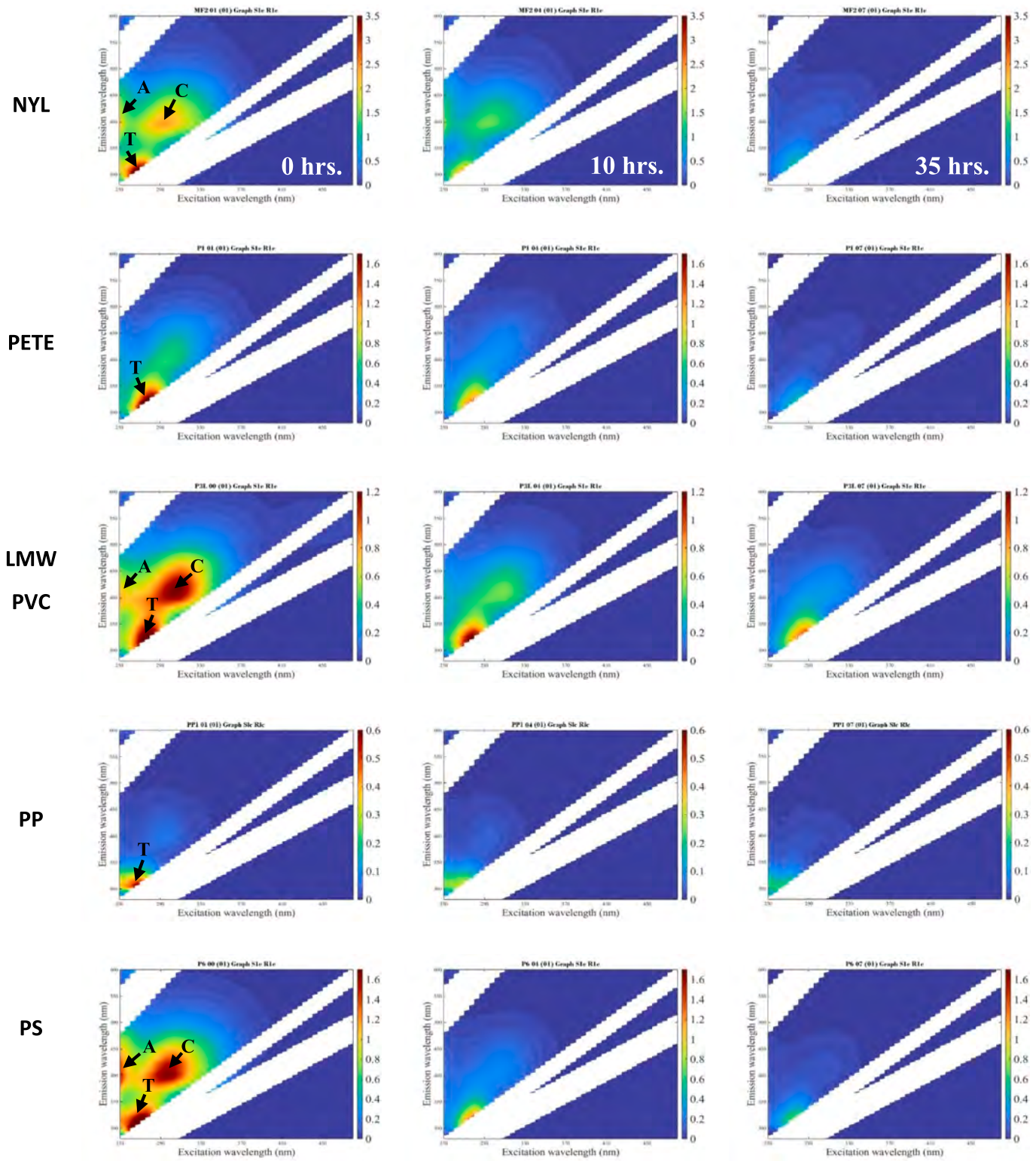

Fig. 3. Examples of fluorescence EEM spectra of plastic-derived DOM from NYL, PS, PETE, PVC, and PP. In addition to initial (0 h) DOM samples (left column), EEMs of time series samples, including 10 h (center) and 35 h (right) UV-exposure, were given to show changes in EEM spectra during photochemical degradation. Major fluorescence peaks A (Ex/Em ≈ 250/400 nm), C (Ex/Em ≈ 325/425 nm), and T (Ex/Em ≈ 275/325 nm) are also identified with corresponding arrows in the initial DOM.

3.4. Molecular size and zeta potential of plastic derived DOM

Surface/colloidal properties reported here for plastic-derived DOM included molecular size and Zeta-potential (Table S2). Molecular sizes of plastic-derived DOM ranged from 60.3 ± 0.8 nm (polyester-DOM) to 937.2 ± 117.8 nm (LDPE-DOM) with large differences between plastic types, although DOM from HDPE were not measurable due to its low DOM abundance (Table S2). The average molecular size of MP-derived DOM was in general larger than that of MF-derived DOM, with exception to PETE (306 ± 7 nm). The average molecular sizes of water-soluble

DOM released from MPs and MFs (Table S2) did not relate to their molar masses of corresponding pristine polymers (Table 1), suggesting that plastic-derived DOM do not simply consist of plastic monomers from original polymers.

Zeta potentials of plastic-derived DOM varied widely (Table S2), ranging from −42.5 ± 1.4 mV to +4.6 ± 0.7 mV. Based on these zeta potentials, all plastic-derived DOM were negatively charged, except for DOM released from LMW-PVC (+4.6 ± 0.7 mV). In addition, zeta potentials from MF-derived DOM were more negative compared to those of MPs-derived DOM samples (Table S2).

Difficulty in measuring average sizes for select MPs under low DOM concentrations, combined with the low zeta potentials, indicate DOM aggregation was actively occurring during measurement in DOM samples from HDPE, HMW-PVC, and PS. Additionally, molecular sizes measured for PS- and LDPE-derived DOM (Table S2) were larger than the pore-size of membrane filters (0.7 μm), further supporting evidential DOM coagulation/aggregation after sample filtration. Overall, MF-derived DOM showed consistently smaller sized, well dispersed, and more stable material compared to MP-derived DOM. Mechanical force can be used to produce nanoplastics from commercial PS products (Ekvall et al., 2019) where the observations of MP PS to nanoplastic styrene were characterized by shape changes, formation of larger aggregates, and near neutral surface charges. Similar properties are seen in leached DOM from this study, suggesting DOM filtrates may not remain as their initial molecular sizes, but are aggregating suspensions of nano and colloidal particles, like those observed for natural DOM (Xu and Guo, 2018).

3.5. Photochemical reactivity of plastic-derived DOM

Changes in DOM concentrations over time during photochemical degradation of plastic-derived DOM are depicted in Fig. 4. Both CDOM and DOC concentrations decreased with time, although to different extents among selected MFs and MPs, indicating that water-soluble DOM released from selected MF and MPs are all photochemically reactive. Specifically, MP-derived DOM showed the greatest decreases totaling 68.6, 61.8, and 90.8 % CDOM and 87.9, 17.9, and 93.9 % DOC loss for PETE, LMW-PVC, and PS, respectively, within 110 h (Fig. 4). Compared to MP-derived DOM, NYL-derived DOM, which had two and a half times the amount of starting CDOM and five times the amount of starting DOC, exhibited only minor decreases of 13.5 % for CDOM and 17.5 % for DOC. As exemplified here, the photochemical reactivity of plastic-derived DOM, or DOM losses, during degradation were largely associated to the type of polymers and less regulated by DOM yields or DOM concentrations.

Based on the degradation time-series data, the degradation rate constants of different plastic-derived DOM (MPs and MF) were estimated for CDOM and DOC using a first-order reaction equation:

$$\frac{dC}{dt} = -kC \text{ or } lnC = lnC_0 - k(t - t_0)$$

where C is concentration of CDOM or DOC, t is time (in hour), and k is degradation rate constant (in $time^{-1}$) or the slope value in the correlation between ln C and t. Linear regressions between ln C and t (Fig. S1) were statistically significant ($p < 0.050$) for all polymers except DOC from LMW-PVC ($p = 0.051$).

Based on their slope values (Fig. S1), the estimated degradation rate constants (k) of both CDOM and DOC for each plastic polymer are listed in Table 2. The degradation rate constants of plastic-derived DOMs varied widely between polymer and DOM type, ranging from 1.0×10^{-3} h^{-1} to 2.2×10^{-2} h^{-1} for CDOM and from 9.0×10^{-4} h^{-1} to 2.0×10^{-2} h^{-1} for DOC. PS-derived DOM had the highest k values for both CDOM and DOC (2.2×10^{-2} h^{-1} and 2.0×10^{-2} h^{-1}, respectively), which are

Table 2
Degradation rate constants and half-lives of water-soluble DOM from selected MPs and MFs, including polyethylene terephthalate (PETE), low molecular weight-polyvinyl chloride (LMW-PVC), polystyrene (PS), and nylon (NYL).

	Degradation Rate Constant (hr^{-1})		*Half-Life (hr)*	
Polymer	CDOM	DOC	CDOM	DOC
PETE	$1.0 \pm 0.05 \times 10^{-2}$	$1.5 \pm 0.02 \times 10^{-2}$	69 ± 3.6	46 ± 1.0
LMW-PVC	$8.7 \pm 0.22 \times 10^{-3}$	$1.6 \pm 0.06 \times 10^{-3}$	80 ± 2.6	433 ± 15
PS	$2.2 \pm 0.13 \times 10^{-2}$	$2.0 \pm 0.01 \times 10^{-2}$	31 ± 2.0	35 ± 3.8
NYL	$1.0 \pm 0.12 \times 10^{-3}$	$9.0 \pm 1.55 \times 10^{-4}$	693 ± 73	770 ± 108

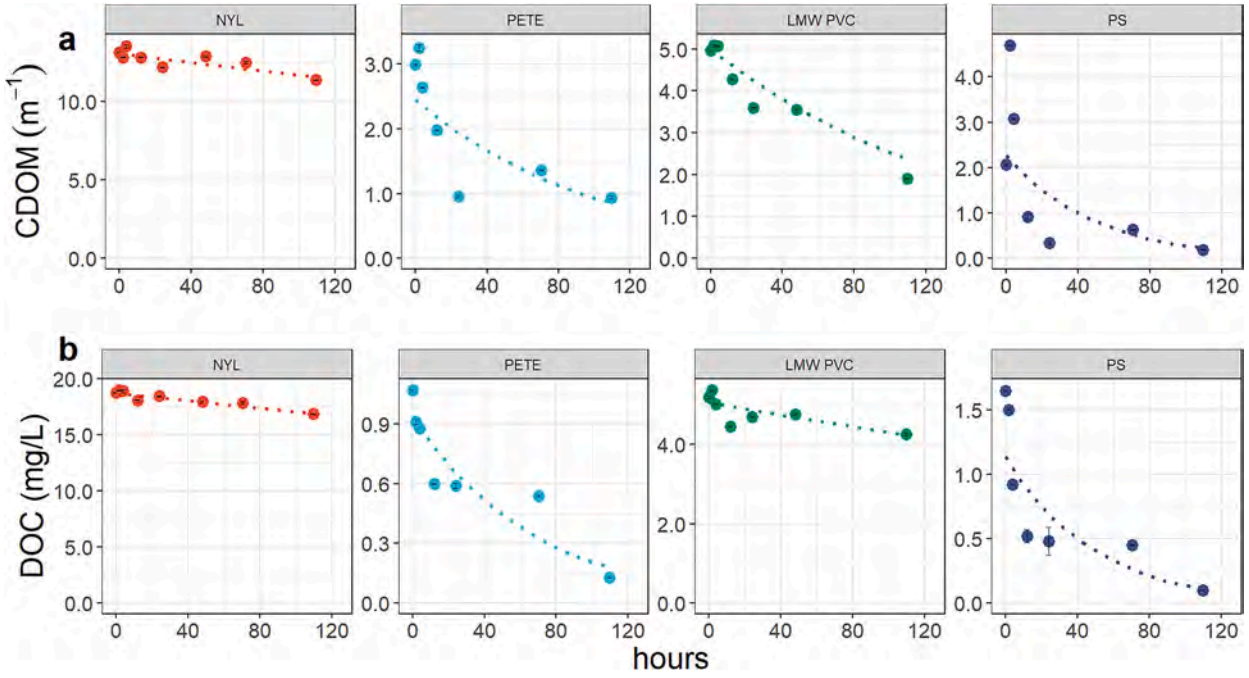

Fig. 4. Variations in CDOM (a) and DOC concentrations (b) with time during photochemical degradation of the four plastic derived water soluble DOM, including nylon, PETE, LMW-PVC, and PS. Error bars for average values represent the standard deviation of replicated measurements.

20 times higher than NYL-derived DOM rates for both CDOM and DOC (1.0×10^{-3} h^{-1} and 9.0×10^{-4} h^{-1}, respectively). As expected, within the bulk DOM pool, CDOM had k values greater than those of bulk DOC, except for PETE which had similar degradation rate constants between CDOM and DOC, likely due to its higher aromaticity ($SUVA_{254}$) and thus a less distinguishable rate constant between CDOM and bulk DOM. Higher degradation rate constants for CDOM indicate that the chromophoric components within the bulk DOM pool were preferentially photochemically degraded compared to non-chromophoric DOM or the bulk DOM pool (Chen and Jaffé, 2016). Results observed here for plastic derived DOM agree well with those observed for natural DOM, with higher photochemical reactivity in aromatic and humic-like components (Chen and Jaffé, 2016; Xu and Guo, 2018).

As shown in Table 2, the degradation rate constants of plastic-derived water-soluble DOM varied significantly depending on the type of polymer and the chemical/optical properties of DOM. The highest degradation rate constants were observed for PS-derived DOM, followed by PETE-, PVC-, and NYL-derived DOM. The corresponding mean half-life in DOM degradation ranged from 31 to 693 h for CDOM and 35 to 770 h for bulk DOC (Table 2), indicating again higher photochemical reactivity for CDOM components compared to the bulk DOC pool. Comparing the DOM yields and photodegradation rate constants, high DOM yield does not necessarily equate to a high photosensitivity. Instead, the photochemical reactivity of plastic-derived DOM is predominantly determined by the chemical/optical properties of DOM and the type of polymers, such as aromatic group containing polymers (e.g., PS and PETE) vs. non-aromatic polymers. In our degradation experiments, all selected MPs and MF (NYL) had higher CDOM yields per unit mass of plastic and higher $SUVA_{254}$ values compared to their counterparts (Figs. 1 and 2). There was a somewhat positive correlation between $SUVA_{254}$ values in the initial DOM and their degradation rate constants (not shown), indicating increasing degradation rate constant with increasing $SUVA_{254}$ in plastic-derived DOM. In fact, $SUVA_{254}$ values predict DOM degradation rate ($R^2 = 0.45$) better than CDOM concentration ($R^2 = 0.13$) although these correlations were not statistically significant at the 0.05 level.

3.6. Variations in chemical and optical properties during DOM degradation

The chemical and optical properties of plastic-derived DOM varied to different extents during degradation (Table S3). In general, $SUVA_{254}$ of the plastic-derived DOM did not show measurable changes compared to initial DOMs (Table S3), suggesting that the degradation of plastic-derived DOM was either somewhat homogeneous, or in the form of entire DOM molecules or monomers. In addition, $S_{275–295}$ values of NYL- and LMW-PVC-derived DOM showed little changes, remaining relatively constant throughout the UV exposure (not shown). However, $S_{275–295}$ values of PETE- and PS-derived DOM were more variable, both expressing a slightly decreasing trend, from 0.0210 to 0.0001 nm^{-1} for PETE and 0.020 to 0.008 nm^{-1} for PS, respectively, indicating an increase in apparent DOM molecular weight (Table S3). As shown in Table 1, both PETE and PS contain aromatic or photochemical responsive functionalities, but the decrease in $S_{275–295}$ value or increase in apparent DOM molecular weight did not seem straightforward. There were likely more active DOM inter-molecular reactions during or after degradation for the two aromatic-containing polymers (PETE and PS), resulting in changes in DOM molecular size after degradation, which is further supported by changes in Zeta-potential and DOM molecular size (Fig. 5).

For example, DOM molecular sizes generally decreased after photochemical degradation in all samples except for PS-derived DOM (Fig. 5). While the size changes were small, the greatest decrease in DOM molecular size was seen in PETE-DOM, with an average of 8.3 % from 277 nm to 254 nm, while PS-DOM increased 37 % in DOM size from 300 nm to 411 nm, likely resulting from coagulation/aggregation. Notably, for DOM released from NYL, PETE, and LMW-PVC, changes in size after degradation did not reach statistical significance ($p > 0.05$). In addition, changes in average sizes and DOM stability can be related to zeta potentials (Wang and Keller, 2009; Xu et al., 2018). Higher zeta potentials

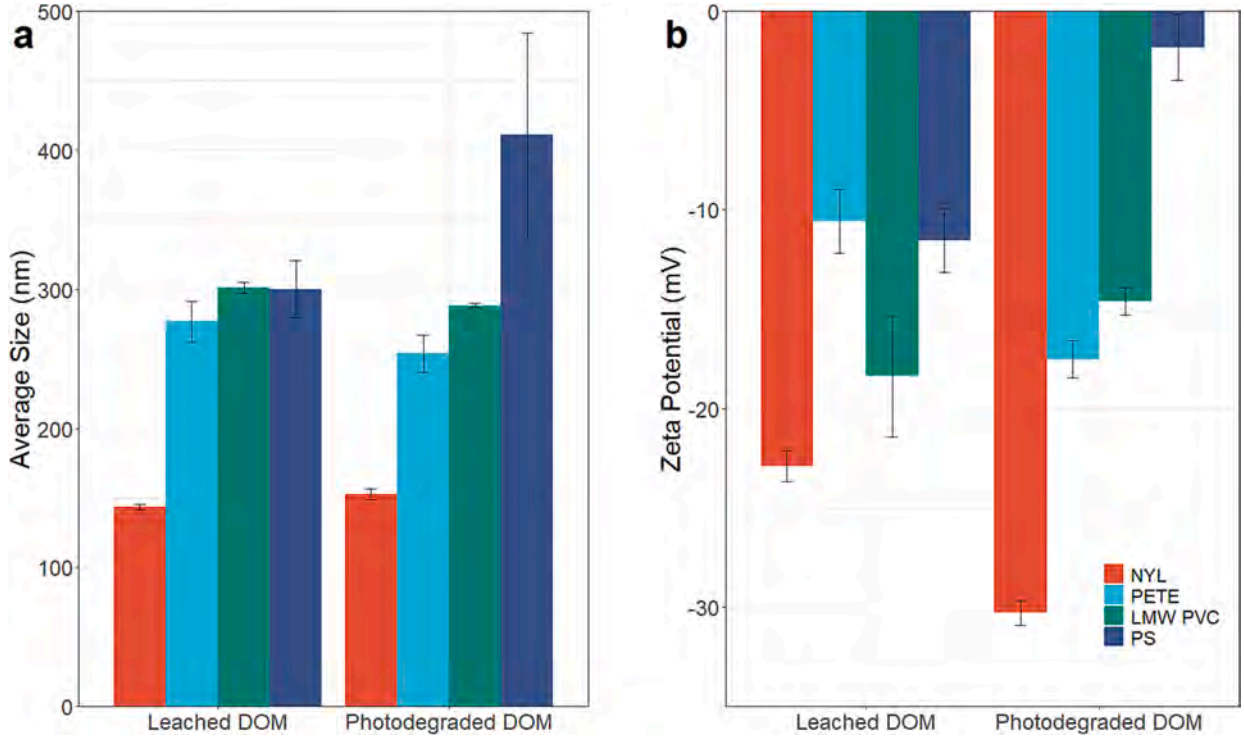

Fig. 5. Variations in DOM molecular size or hydrodynamic diameter (a) and Zeta potential (b) of plastic-derived DOM before and after UV exposure for selected polymers (Error bars represent the standard deviation of replicated measurements).

(absolute values) typically lead to increased electrostatic repulsion between particles or DOM molecules, preventing aggregation and maintaining smaller sizes. Zeta potential increases after exposure were significant in NYL-DOM ($p = 0.006$) and PETE-DOM ($p = 0.037$) samples while PS-DOM resulted in a significant ($p = 0.007$) reduction in zeta potential or decreasing stability (Fig. 5b). LMW-PVC exhibited a decrease in size after photodegradation but was not significant ($p > 0.05$). PS-DOM had the greatest change in zeta potential after degradation, decreasing 82 % from −11.5 mV to −1.8 mV. The change in zeta potential observed for degraded DOM from PS supports the increase in DOM size measured by DLS (Fig. 5). PS-derived DOM seemed to experience rapid phase transformation from dissolved to aggregated macromolecules or nanoparticles.

Consistent with the decrease in both CDOM and DOC during photochemical degradation, fluorescence EEM of plastic-derived DOM exhibited evidential decreases in fluorescence intensities after UV-irradiation (Fig. 3). All selected MP- and MF-derived DOM demonstrated progressive decreases in fluoresce intensity in all major fluorescent peaks, especially in peaks A and C after 35 h of UV-irradiation (Fig. 3). These results are again consistent with those observed for natural DOM in the environment, with humic-like DOM components preferentially degraded by photochemical processes (Chen and Jaffé, 2016; Hansen et al., 2016).

In addition to changes in fluorescence spectra, other derived optical properties, such as HIX values, demonstrated a consistent decrease during degradation, especially for PS-, PETE- and PVC-derived DOM (Table S1). For example, values of HIX decreased 73 % from 0.84 in the initial solution, to 0.33 after 10 h and to 0.23 after 35 h of UV-irradiation for PS-derived DOM, 52 % from 0.84 to 0.49 and to 0.40 for LMW-PVC-derived DOM, and 17 % from 0.41 to 0.37 and 0.34 for PETE-derived DOM. Decreases in HIX support preferential degradation of humified DOM components during photochemical degradation.

Our results align with previous investigation into DOM degradation in the environment. For example, Zhuang et al. (2022) reported the impacts on HIX values from varying environmental sources such as plant leachate, wastewater, leaf litter, and river waters. Their study clearly demonstrated the preferential photodegradation of humic-like components and higher degradability of aromatic sources like leaf litter. HIX values exhibited minimal change after degradation for plant leachate, but decreased up to 71 % for leaf litter and 40–61 % for other sources. This underscores the relationship between initial HIX values and the degree of degradation, where lower initial HIX values correlate with lower degradation of HIX values after exposure to UV radiation. While photochemical degradation is examined here, further studies are needed to explore the biological reactivity of plastic-derived DOM in the environment and the impact of ionic strength and water matrix on the leaching of DOM from different plastic polymers and additives under pristine and weathered conditions.

3.7. Environmental significance

The results reported here highlight the environmental relevance of plastic-derived DOM in aquatic processes. The significance should not be understated, as many of the plastics investigated here are common in everyday products. For example, nylon has significant potential to leach large amounts of DOM, up to one thousand times more than MPs, that can exist in the environment for long periods of time due to its high photochemical resistance. The importance is amplified by nylon's prevalence as a common consumer product and its high loads to wastewater treatment plants and eventual wastewater sludges (Liu et al., 2019; Murphy et al., 2016). When evaluating the impact of plastic pollution on aquatic ecosystems, plastic derived DOM must be taken into consideration since DOM can have a range of effects on biogeochemical and environmental processes (Lee and Hur, 2021; Li et al., 2023). In contrast to nylon, the degradation of PP debris could release DOM, but has overall low DOM yields for each gram of plastic and is relatively resistant to photodegradation. However, PP is also extremely prevalent in consumer products, especially through the production of disposable face masks during the COVID-19 pandemic (O'Dowd et al., 2020; Statista, 2022).

While NYL can be impacted by microbial degradation (Kanagawa et al., 1989; Kinoshita et al., 1975; Kulkarni and Kanekar, 1998), PP shows resistance and is minimally degraded (Artham et al., 2009). Other plastics like PETE and PS have higher resistance to microbial attack (Müller et al., 2001; Pushpadass et al., 2010), but are extremely photochemically responsive. The results of this study should be used in conjunction with microbial studies to target which plastics are most susceptible to long term plastic pollution and which plastics to target for removal from production first.

4. Conclusions

We have evaluated the DOM leaching potential for seven microplastics and three microfibers, characterized the chemical and optical properties of plastic-derived DOM, and uncovered the photochemical reactivity of DOM released from NYL, LMW-PVC, PETE, and PS. Main conclusions are as follows.

- Yields of water-soluble DOM per unit mass of MPs were related to their inherent polymer's structures following the order of PETE >PVC > PS > HDPE >LDPE >PP. In addition, PS-derived DOM seemed to experience rapid phase transformation from dissolved to aggregated macromolecules or nanoparticles.
- Microfibers, regardless of type, leach a magnitude of 10–1000 times more DOM than the MPs. MFs-derived DOM contained small-sized, highly negatively charged, or stable molecules, which differ from those found in DOM released by MPs.
- DOM released from MPs containing aromatic structures, such as PETE and PS, exhibited high $SUVA_{254}$ values or aromaticity. Conversely, high CDOM yields from MFs did not lead to high $SUVA_{254}$ in MF-derived DOM.
- Plastic-derived DOM exhibited fluorescence peaks resembling peaks C, A and T, particularly noticeable in DOM released from NYL, LMW-PVC, PETE, PP, and PS. The photochemical reactivity of plastic-derived DOM was evident through changes of fluorescence spectra during UV irradiation.
- The degradation rate constant of plastic-derived DOM varied widely among the selected MPs and microfibers, with noticeably low in NYL-derived DOM but high in PETE- and PS-derived DOM. In general, DOM released from aromatic polymers had high degradation potentials, while DOM from nonaromatic polymers, such as PP and NYL, were more photochemically resistant.

Declaration of competing interest

The authors declare that they have no known competing financial interests or personal relationships that could have appeared to influence the work reported in this paper.

Data availability

Data will be made available on request.

Acknowledgements

We gratefully thank Hui Lin and Eric Ostovich for their technical assistance during sample analysis and four anonymous reviewers for their constructive comments, which greatly improved the manuscript. This work was supported in part by the National Science Foundation (NSF award # 2204145), Discovery and Innovation *Grant* Program (DIG) from University of Wisconsin-Milwaukee (101X405 and 101X439), and Freshwater Collaborative of Wisconsin (through funding

from UW-System and WEDC). S.M.K. acknowledges support from Egyptian Government Scholarship - The Cultural Affairs and Mission Sectors of the Egyptian Ministry of Higher Education.

Appendix A. Supplementary data

Supplementary data to this article can be found online at https://doi.org/10.1016/j.scitotenv.2023.168616.

References

Ahmed, A.S.S., Billah, M.M., Ali, M.M., Bhuiyan, M.K.A., Guo, L., Mohinuzzaman, M., et al., 2023. Microplastics in aquatic environments: a comprehensive review of toxicity, removal, and remediation strategies. Sci. Total Environ. 876, 162414.

Artham, T., Sudhakar, M., Venkatesan, R., Madhavan Nair, C., Murty, K.V.G.K., Doble, M., 2009. Biofouling and stability of synthetic polymers in sea water. Int. Biodeter. Biodegr. 63, 884–890.

Ateia, M., Ersan, G., Alalm, M.G., Boffito, D.C., Karanfil, T., 2022. Emerging investigator series: microplastic sources, fate, toxicity, detection, and interactions with micropollutants in aquatic ecosystems – a review of reviews. Environ. Sci.: Processes Impacts 24, 172–195.

Boldrini, A., Galgani, L., Consumi, M., Loiselle, S.A., 2021. Microplastics contamination versus inorganic particles: effects on the dynamics of marine dissolved organic matter. Environments 8.

Cai, L., Wang, J., Peng, J., Wu, Z., Tan, X., 2018. Observation of the degradation of three types of plastic pellets exposed to UV irradiation in three different environments. Sci. Total Environ. 628-629, 740–747.

Chen, M., Jaffé, R., 2016. Quantitative assessment of photo- and bio-reactivity of chromophoric and fluorescent dissolved organic matter from biomass and soil leachates and from surface waters in a subtropical wetland. Biogeochemistry 129, 273–289.

Chen, M., Xu, J., Tang, R., Yuan, S., Min, Y., Xu, Q., et al., 2022. Roles of microplastic-derived dissolved organic matter on the photodegradation of organic micropollutants. J. Hazard. Mater. 440, 129784.

Coble, P.G., 2007. Marine optical biogeochemistry: the chemistry of ocean color. Chem. Rev. 107, 402–418.

Cózar, A., Martí, E., Duarte, C.M., García-de-Lomas, J., van Sebille, E., Ballatore, T.J., et al., 2017. The Arctic Ocean as a dead end for floating plastics in the North Atlantic branch of the thermohaline circulation. Sci. Adv. 3, e1600582.

Decker, C., 1984. Photodegradation of PVC. In: Owen, E.D. (Ed.), Degradation and Stabilisation of PVC. Springer, Netherlands, Dordrecht, pp. 81–136.

DeVilbiss, S.E., Zhou, Z., Klump, J.V., Guo, L., 2016. Spatiotemporal variations in the abundance and composition of bulk and chromophoric dissolved organic matter in seasonally hypoxia-influenced Green Bay, Lake Michigan, USA. Sci. Total Environ. 565, 742–757.

Eerkes-Medrano, D., Thompson, R.C., Aldridge, D.C., 2015. Microplastics in freshwater systems: a review of the emerging threats, identification of knowledge gaps and prioritisation of research needs. Water Res. 75, 63–82.

Ekvall, M.T., Lundqvist, M., Kelpsiene, E., Šileikis, E., Gunnarsson, S.B., Cedervall, T., 2019. Nanoplastics formed during the mechanical breakdown of daily-use polystyrene products. Nanoscale Adv. 1, 1055–1061.

Forum, W.E., Company, EmFaM, 2016. The New Plastics Economy — Rethinking the Future of Plastics.

Gago, J., Carretero, O., Filgueiras, A.V., Viñas, L., 2018. Synthetic microfibers in the marine environment: a review on their occurrence in seawater and sediments. Mar. Pollut. Bull. 127, 365–376.

Gewert, B., Plassmann, M.M., MacLeod, M., 2015. Pathways for degradation of plastic polymers floating in the marine environment. Environ. Sci.: Processes Impacts 17, 1513–1521.

Gewert, B., Plassmann, M., Sandblom, O., MacLeod, M., 2018. Identification of chain scission products released to water by plastic exposed to ultraviolet light. Environ. Sci. Technol. Lett. 5, 272–276.

Geyer, R., Jambeck, J.R., Law, K.L., 2017. Production, use, and fate of all plastics ever made. Sci. Adv. 3, e1700782.

Gillibert, R., Balakrishnan, G., Deshoules, Q., Tardivel, M., Magazzù, A., Donato, M.G., et al., 2019. Raman tweezers for small microplastics and nanoplastics identification in seawater. Environ. Sci. Technol. 53, 9003–9013.

Gunaalan, K., Nielsen, T.G., Rodríguez Torres, R., Lorenz, C., Vianello, A., Andersen, C. A., Vollertsen, J., Almeda, R., 2023. Is zooplankton an entry point of microplastics into the marine food web? Environ. Sci. Technol. 57, 11643–11655.

Hansen, A.M., Kraus, T.E.C., Pellerin, B.A., Fleck, J.A., Downing, B.D., Bergamaschi, B.A., 2016. Optical properties of dissolved organic matter (DOM): effects of biological and photolytic degradation. Limnol. Oceanogr. 61, 1015–1032.

Helms, J.R., Stubbins, A., Ritchie, J.D., Minor, E.C., Kieber, D.J., Mopper, K., 2008. Absorption spectral slopes and slope ratios as indicators of molecular weight, source, and photobleaching of chromophoric dissolved organic matter. Limnol. Oceanogr. 53, 955–969.

Hendrickson, E., Minor, E.C., Schreiner, K., 2018. Microplastic abundance and composition in Western Lake superior as determined via microscopy, Pyr-GC/MS, and FTIR. Environ. Sci. Technol. 52, 1787–1796.

Huguet, A., Vacher, L., Relexans, S., Saubusse, S., Froidefond, J.M., Parlanti, E., 2009. Properties of fluorescent dissolved organic matter in the Gironde Estuary. Org. Geochem. 40, 706–719.

Kanagawa, K., Negoro, S., Takada, N., Okada, H., 1989. Plasmid dependence of Pseudomonas sp. strain NK87 enzymes that degrade 6-aminohexanoate-cyclic dimer. J. Bacteriol. 171, 3181–3186.

Kanhai, L.D.K., Gardfeldt, K., Krumpen, T., Thompson, R.C., O'Connor, I., 2020. Microplastics in sea ice and seawater beneath ice floes from the Arctic Ocean. Sci. Rep. 10, 5004.

Kinoshita, S., Kageyama, S., Iba, K., Yamada, Y., Okada, H., 1975. Utilization of a cyclic dimer and linear oligomers of ε-Aminocaproic acid by Achrornobacter guttatus KI 72. Agric. Biol. Chem. 39, 1219–1223.

Kteeba, S.M., El-Adawi, H.I., El-Rayis, O.A., El-Ghobashy, A.E., Schuld, J.L., Svoboda, K. R., et al., 2017. Zinc oxide nanoparticle toxicity in embryonic zebrafish: mitigation with different natural organic matter. Environ. Pollut. 230, 1125–1140.

Kulkarni, R.S., Kanekar, P.P., 1998. Bioremediation of epsilon-caprolactam from nylon-6 waste water by use of Pseudomonas aeruginosa MCM B-407. Curr. Microbiol. 37, 191–194.

Lee, Y.K., Hur, J., 2021. Adsorption of microplastic-derived organic matter onto minerals. Water Res. 187, 16426.

Lee, Y.K., Murphy, K.R., Hur, J., 2020. Fluorescence signatures of dissolved organic matter leached from microplastics: polymers and additives. Environ. Sci. Technol. 54, 11905–11914.

Lee, Y.K., Hong, S., Hur, J., 2021. Copper-binding properties of microplastic-derived dissolved organic matter revealed by fluorescence spectroscopy and two-dimensional correlation spectroscopy. Water Res. 190, 116775.

Lenaker, P.L., Corsi, S.R., Mason, S.A., 2021. Spatial distribution of microplastics in surficial benthic sediment of Lake Michigan and Lake Erie. Environ. Sci. Technol. 55, 373–384.

Leslie, H.A., van Velzen, M.J.M., Brandsma, S.H., Vethaak, A.D., Garcia-Vallejo, J.J., Lamoree, M.H., 2022. Discovery and quantification of plastic particle pollution in human blood. Environ. Int. 163, 107199.

Li, D., Lin, H., Guo, L., 2023. Comparisons in molecular weight distributions and size-dependent optical properties among model and reference natural dissolved organic matter. Environ. Sci. Pollut. Res. 30, 57638–57652.

Lim, X., 2021. Microplastics are everywhere—but are they harmful. Nature 593, 22–25.

Lin, H., Guo, L., 2020. Variations in colloidal DOM composition with molecular weight within individual water samples as characterized by flow field-flow fractionation and EEM-PARAFAC analysis. Environ. Sci. Technol. 54, 1657–1667.

Lin, H., Xu, H., Cai, Y., Belzile, C., Macdonald, R.W., Guo, L., 2021. Dynamic changes in size-fractionated dissolved organic matter composition in a seasonally ice-covered Arctic River. Limnol. Oceanogr. 66, 3085–3099.

Liu, X., Yuan, W., Di, M., Li, Z., Wang, J., 2019. Transfer and fate of microplastics during the conventional activated sludge process in one wastewater treatment plant of China. Chem. Eng. J. 362, 176–182.

Müller, R.J., Kleeberg, I., Deckwer, W.D., 2001. Biodegradation of polyesters containing aromatic constituents. J. Biotechnol. 86, 87–95.

Murphy, F., Ewins, C., Carbonnier, F., Quinn, B., 2016. Wastewater treatment works (WwTW) as a source of microplastics in the aquatic environment. Environ. Sci. Technol. 50, 5800–5808.

Napper, I.E., Thompson, R.C., 2020. Plastic debris in the marine environment: history and future challenges. Global Chall. 4, 1900081.

O'Dowd, K., Nair, K.M., Forouzandeh, P., Mathew, S., Grant, J., Moran, R., et al., 2020. Face masks and respirators in the fight against the COVID-19 pandemic: a review of current materials. Adv. Futur. Perspect. Mater. (Basel) 13.

OECD, 2022. Global Plastics Outlook.

Osburn, C., Wigdahl-Perry, C., Fritz, S., Saros, J., 2011. Dissolved organic matter composition and photoreactivity in lakes of the US Great Plains. Limnol. Oceanogr. 56, 2371–2390.

Park, J., Goh, M., Akagi, K., 2014. Helical nylons and polyphthalamides synthesized by chiral interfacial polymerizations between chiral Nematic liquid crystal and water layers. Macromolecules 47, 2784–2795.

Piyawardhana, N., Weerathunga, V., Chen, H.-S., Guo, L., Huang, P.-J., Ranatunga, R.R. M.K.P., et al., 2022. Occurrence of microplastics in commercial marine dried fish in Asian countries. J. Hazard. Mater. 423, 127093.

Pushpadass, H.A., Weber, R.W., Dumais, J.J., Hanna, M.A., 2010. Biodegradation characteristics of starch-polystyrene loose-fill foams in a composting medium. Bioresour. Technol. 101, 7258–7264.

Romera-Castillo, C., Pinto, M., Langer, T.M., Álvarez-Salgado, X.A., Herndl, G.J., 2018. Dissolved organic carbon leaching from plastics stimulates microbial activity in the ocean. Nat. Commun. 9, 1430.

Romera-Castillo, C., Mallenco-Fornies, R., Saá-Yánez, M., Álvarez-Salgado, X.A., 2022. Leaching and bioavailability of dissolved organic matter from petrol-based and biodegradable plastics. Mar. Environ. Res. 176, 105607.

Singh, R.P., Mishra, S., Das, A.P., 2020. Synthetic microfibers: pollution toxicity and remediation. Chemosphere 257, 127199.

Statista, 2022. Market Volume of Polypropylene Worldwide From 2015 to 2021, With a Forecast for 2022 to 2029. 2023.

Stubbins, A., Law, K.L., Muñoz, S.E., Bianchi, T.S., Zhu, L., 2021. Plastics in the Earth system. Science 373, 51–55.

Sun, Q., Li, J., Wang, C., Chen, A., You, Y., Yang, S., et al., 2022. Research progress on distribution, sources, identification, toxicity, and biodegradation of microplastics in the ocean, freshwater, and soil environment. Front. Environ. Sci. Eng. 16, 1.

van Wezel, A., Caris, I., Kools, S.A.E., 2016. Release of primary microplastics from consumer products to wastewater in the Netherlands. Environ. Toxicol. Chem. 35, 1627–1631.

Walsh, A.N., Reddy, C.M., Niles, S.F., McKenna, A.M., Hansel, C.M., Ward, C.P., 2021. Plastic formulation is an emerging control of its photochemical fate in the ocean. Environ. Sci. Technol. 55, 12383–12392.

Wang, P., Keller, A.A., 2009. Natural and engineered nano and colloidal transport: role of zeta potential in prediction of particle deposition. Langmuir 25, 6856–6862.
Weber, J.N., 2011. Polyamides. Kirk-Othmer Encyclopedia of Chemical Technology, pp. 1–63.
Weishaar, J.L., Aiken, G.R., Bergamaschi, B.A., Fram, M.S., Fujii, R., Mopper, K., 2003. Evaluation of specific ultraviolet absorbance as an indicator of the chemical composition and reactivity of dissolved organic carbon. Environ. Sci. Technol. 37, 4702–4708.
Xu, H., Guo, L., 2018. Intriguing changes in molecular size and composition of dissolved organic matter induced by microbial degradation and self-assembly. Water Res. 135, 187–194.
Xu, H., Lin, H., Jiang, H., Guo, L., 2018. Dynamic molecular size transformation of aquatic colloidal organic matter as a function of pH and cations. Water Res. 144, 543–552.
Zhou, Z., Guo, L., Shiller, A.M., Lohrenz, S.E., Asper, V.L., Osburn, C.L., 2013. Characterization of oil components from the Deepwater horizon oil spill in the Gulf of Mexico using fluorescence EEM and PARAFAC techniques. Mar. Chem. 148, 10–21.
Zhou, Z., Guo, L., Minor, E.C., 2016. Characterization of bulk and chromophoric dissolved organic matter in the Laurentian Great Lakes during summer 2013. J. Great Lakes Res. 42, 789–801.
Zhu, L., Zhao, S., Bittar, T.B., Stubbins, A., Li, D., 2020. Photochemical dissolution of buoyant microplastics to dissolved organic carbon: rates and microbial impacts. J. Hazard. Mater. 383, 121065.
Zhuang, W.-E., Chen, W., Yang, L., 2022. Effects of photodegradation on the optical indices of chromophoric dissolved organic matter from typical sources. Int. J. Environ. Res. Public Health 19.